Proceedings of the ASME 2017 Conference on Smart Materials, Adaptive Structures, and Intelligent Systems
SMASIS 2017
September 18-20, 2017, Snowbird, UT, USA

SMASIS2017-3844

DYNAMIC MODELING OF TRIBOELECTRIC GENERATORS USING LAGRANGE'S EQUATION

Sean Gauntt
Department of Mechanical and Aeronautical Engineering
Clarkson University
Potsdam, New York 13699
Email: gaunttsm@clarkson.edu

Gregory Batt
Food, Nutrition, and Packaging Sciences Department
Clemson University
Clemson, South Carolina 29634
Email: gbatt@clemson.edu

James Gibert*
Advanced Dynamics and Mechanics Labs (ADAMS)
School of Mechanical Engineering
Purdue University
West Lafayette, Indiana 47907
Email: jgibert@purdue.edu

ABSTRACT

Electret based energy scavenging devices utilize electrostatic induction to convert mechanical energy into electrical energy. Uses for these devices include harvesting ambient energy in the environment and acting as sensors for a range of applications. These types of devices have been used in MEMS applications for over a decade. However, recently there is an interest in triboelectric generators/harvesters, i.e., electret based harvesters that utilize triboelectrification as well as electrostatic induction. The literature is filled with a variety of designs for the latter devices, constructed from materials ranging from paper and thin films; rendering the generators lightweight, flexible and inexpensive. However, most of the design of these devices is ad-hoc and not based on exploiting the underlying physics that govern their behavior; the few models that exist neglect the coupled electromechanical behavior of the devices. Motivated by the lack of a comprehensive dynamic model of these devices this manuscript presents a generalized framework based on a Lagrangian formulation to derive electromechanical equation for a lumped parameter dynamic model of an electret-based harvester. The framework is robust, capturing the effects of traditional MEMS devices as well as triboelectric generators. Exploiting numerical simulations the predictions are used to examine the behavior of electret based devices for a variety of loading conditions simulating real-world applications such as power scavengers under simple harmonic forcing and in pedestrian walking.

NOMENCLATURE

A	surface area
$C_s(x)$	capacitance as a function of displacement for single dielectric
$C_d(x)$	capacitance as a function of displacement for dual dielectric
C_0	initial capacitance
E_n	electric field of the n^{th} dielectric material
Q_0	initial total charge of the n^{th} dielectric material
Q_n	capacitance as a function of displacement
R	load resistance
T	kinetic energy
U	Rayleigh dissipation function
V	potential energy
c_{eq}	total damping coefficient of system
f	applied load
g	gravitational constant
k_{eq}	equivalent stiffness of system
m	mass of upper electrode
q	induced charge on the electrodes

*Address all correspondence to this author.

q_r	generalized coordinates
x	perturbation displacement of upper electrode
x_{eq}	equilibrium displacement
x_t	total displacement of upper electrode
ρ	charge density
ε_n	permittivity of the n^{th} material
ζ	damping ratio
σ_n	surface charge density on n^{th} surface
ω_n	natural frequency of the system
Ω	forcing frequency
ϕ	phase constant

INTRODUCTION

Mechanical energy harvesting has been of great interest to the engineering community over the last few years. Vibrational energy harvesting converts vibrations (mechanical energy) in the environment into electrical power [1]. These devices utilize a transduction mechanism to generate an electric potential due to mechanical stimuli. Three common transduction mechanisms are: piezoelectricity, electromagnetism, and electrostaticity [1]. The discussion is restricted to only electrostatic devices. Electrostatic devices are based on a variable capacitive structure and there are two types, electret-free or electret-based devices [1]. An electret is an electrical insulator or dielectric that holds a semi-permanent charge [2]. Electrets are the source of an electric field within the capacitive structure of these devices [3]. This research focuses on contact mode triboelectric generators, which are a form of electret based electrostatic devices. Their function depends on contact electrification and electrostatic induction [4]. The movement of two electrodes relative to each other and to a charged electret results in electrostatic induction, i.e. an induced charge on the electrodes. As the relative positions of the electrodes change the distribution of the induced charges, the electric field and the total capacitance between the electrodes change, resulting in an electric potential difference between the electrodes [3]. Contact mode triboelectric generators (TGs) have numerous applications both as power sources and as active sensors [4]. Few models for triboelectric generators exist in the literature [3, 4]. This manuscript provides the governing electromechanical equations for a lumped parameter analysis using Lagrange's Equation. These equations are then used in simulations with a variety of forcing functions to illustrate the efficacy of the formulation.

Electrelets

The electrets used in electrostatic devices are charged through the use of triboelectricity [5], a form of static electricity. The term triboelectricity literally means,"electricity generated by friction." Through the use of the triboelectric effect, or contact electrification through the use of friction, materials that behave as electrical insulators become charged with a semi-permanent charge that can last for several years or more depending on the material [2]. Different materials will develop different charges. Several materials are arranged on the triboelectric series (Fig. 1), to show how different materials behave when acted on by the triboelectric effect. The series is organized from materials that develop a strong positive charge to those that develop a strong negative charge. When two materials on this list are put in intimate contact, the higher one on the list will develop a positive charge and the lower will develop a negative charge. Teflon or PTFE and polyethylene are two of the most electronegative materials [5] and are good choices for an electret.

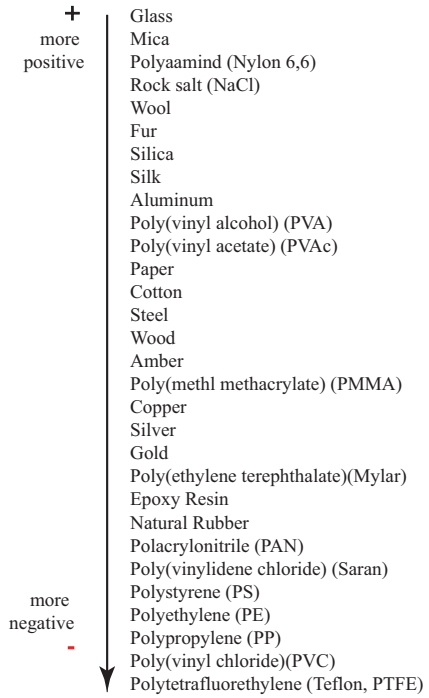

FIGURE 1. TRIBOELECTRIC SERIES.

Triboelectric Generators and Nanogenerators

One of the most interesting designs of contact mode triboelectric generators are those that are made out of paper. They are inexpensive, lightweight, flexible and have the potential to be used for a variety of applications. Karagozler et al. [3] developed a paper energy harvester for the use in interactive children?s books. Several different designs were created to harvest energy from different motions. Only the contact mode generators are of interest here. Their design utilizes a semi-permanent charge on the surface of a sheet of PTFE due to its high electronegativity when charged. The PTFE was charged by rubbing it with newspaper. The PTFE was then attached to a piece of silver coated

polyester (Mylar) that acts as an electrode. Mylar and metals also develop a strong positive charge when charged. Another piece of silver coated polyester was used as a second electrode above the PTFE leaving an air gap between the two. Both electrodes were mounted to pieces of commercial printer paper for added strength and protection.

The previous discussion focused on tribolectric generators. The performance of these devices can be increased by applying surface treatment in the form of adding nanostructures to dielectric material to increase the surface charge. This treatment is usually done to increase surface area of the dielectric, increasing its capability to hold charge. While there are numerous devices that utilize this principle [6, 7, 8, 9]; the next paragraphs provide a limited over view of these devices. Zhong et al. [10] developed a generator utilizes a polyethylene film as the electret, since it has a high electronegativity when charged, and uses carbon nanotubes for the electrode material. The carbon nanotubes were deposited evenly onto a transparent nanopaper. Nanopaper was used to develop a flexible and transparent device. The electret was charged using the corona discharge method. Zhang et al. [11] also developed their own triboelectric generator that utilizes paper. This design uses indium tin oxide for the electrodes and uses polyethylene terephthalate film for the electret. The indium tin oxide was deposited onto two sheets of commercial printing paper. Then a polyethylene sheet was adhered to one of the sheets of paper. The two pieces were then assembled so that the polyethylene of the one sheet was facing the indium tin oxide of the other sheet. This design was intended for use in books or other paper products to harvest energy whenever the pages come in contact or move relative to one another. This design also utilizes a sliding mode that produces energy as the electrodes slide along one another.

Fan et al. [12] developed a contact mode paper generator that is ultra thin and rollable to harvest acoustic energy with potential use in cell phones to harvest energy from human speaking. Multi-holed paper was used for the structural strength of the generator. This was coated with copper, which was used as the electrode material. This design also utilizes a PTFE membrane as the electret material. Paper was chosen for its flexibility, lightweight, low cost and because it is biodegradable [12].

Yang et al. [13] have developed a paper generator in the shape of a slinky that is capable of harvesting energy in many directions and from various forms of human motion, such as stretching, lifting and twisting. These generators utilize aluminum as the electrode material and PTFE as the electret and are constructed of several devices connected in parallel. Few of the generators described above have a mathematical model to accompany the experimental data. The model that was created [3] neglects the mechanical dynamics of the system, only illustrating the electrical components. Only recently work by have considered both the electromechanical coupling in the system [14].

MATHEMATICAL MODEL

The models presented here are for contact mode triboelectric generators [15] and are based on the formulation from [16]. They are derived using Lagrange's Equation, Eq. (1), shown below in terms of the generalized coordinate (q_r), and their time derivatives ($\dot{q}_r$)

$$\frac{d}{dt}\left(\frac{\partial L}{\partial \dot{q}_r}\right) - \frac{\partial L}{\partial q_r} + \frac{\partial U}{\partial \dot{q}_r} = f_r. \tag{1}$$

L is the Lagrangian and can be written as

$$L = T - V, \tag{2}$$

where T is the kinetic energy and V is the potential energy. U is the Rayleigh dissipation function. The next sections present the appropriate expressions for the kinetic and potential energy, and Rayleigh dissipation function for two configurations of contact mode triboelectric generators.

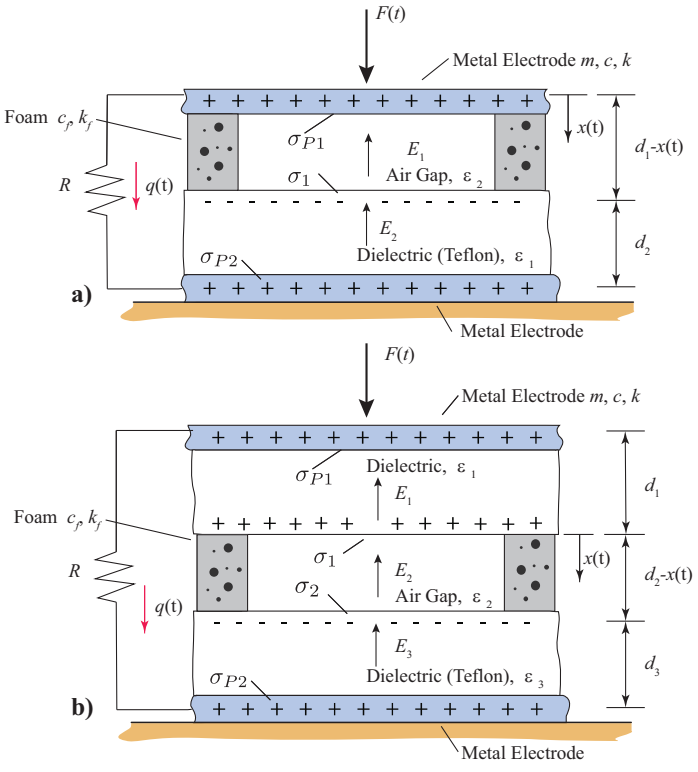

FIGURE 2. SECTION OF CONTACT TRIBOELECTRIC GENERATORS: A) SINGLE DIELECTRIC, B) DOUBLE DIELECTRIC.

Contact Mode Triboelectric Generators

This section presents lumped parameter models of two triboelectric generators: one device containing one dielectric layers and one containing two dielectric layers, Fig. 2. In order to write a lumped parameter approximation of the TGs the generalized coordinates are the total displacement of the upper electrode (x_T) and the electrical displacement in bottom dielectric (q_T).

Equations of Motion for Single Dielectric Generator

The kinetic energy of the TG shown in Fig. a) in terms of the mass (m) and the velocity of the upper electrode ($\dot{x}_T$) can be written as

$$T = \frac{1}{2} m \dot{x}_T. \tag{3}$$

The potential energy of the system is given in terms of the equivalent stiffness of the system(k_{eq}), the mass (m) and the total displacement (x_T) of the upper electrode, acceleration due to gravity (g), the surface area of the generator (A), and the thickness (d_i), the electric field strength(E_i) and permittivity (ε_i) of the various dielectric layers

$$\begin{aligned} V =& \frac{1}{2} k_{eq} x_T^2 + \frac{1}{2} A \left(\varepsilon_1 E_1^2 (d_1 - x_T) + \varepsilon_2 E_2^2 d_2 \right) \\ &+ mg(d_2 + d_1 - x_T). \end{aligned} \tag{4}$$

Finally, the Rayleigh dissipation function for the TG can be written in terms of the velocity of the system, the equivalent damping coefficient of the system (c_{eq}), the load resistance (R), and the current ($\dot{q}_T$),

$$U = \frac{1}{2} c_{eq} \dot{x}_T + \frac{1}{2} R \dot{q}_T. \tag{5}$$

Before this equation can be used in Eq. (1) the potential energy must be written in terms of the the total displacement (x_T) and the total charge (q_T). This is accomplished by using Gauss's law, to convert the electric field strengths to surface charge density (σ),

$$\oint \varepsilon E dA = \sigma. \tag{6}$$

Now, the charge density is uniform over a planar surface bounded by homogenous media, the integral in becomes the product of the integral for the two media on either side of the surface. Using Eq. (6) allows the electric field strength in terms of the surface charge density. This allows the potential energy to be written as

$$\begin{aligned} V =& \frac{1}{2} k_{eq} x_T^2 + \frac{1}{2} A \left(\frac{(\sigma_1 + \sigma_{p2})^2}{\varepsilon_1} (d_1 - x_T) + \frac{\sigma_{p2}^2 d_2}{\varepsilon_2} \right) \\ &+ mg(d_2 + d_1 - x_T). \end{aligned} \tag{7}$$

Equations (3), (5), and (7) are then substituted into Eq. (1) using a load, f, for the mechanical system and no load for electrical system to yield:

$$m\ddot{x}_T + c_{eq}\dot{x}_T + k_{eq} x_T - \frac{A}{2\varepsilon_1} \left(\sigma_1 + \frac{q_T}{A} \right)^2 = f + mg, \tag{8}$$

$$R\dot{q}_T + \frac{q_T}{A} \left(\frac{d_1}{\varepsilon_1} + \frac{d_2}{\varepsilon_2} - \frac{x_T}{\varepsilon_1} \right) + \frac{\sigma_1}{\varepsilon_1} (d_1 - x_T) = 0. \tag{9}$$

Equations around Equilibrium Points for Single Dielectric

In examining small oscillation, the displacement and charge can be written as

$$\begin{aligned} x_T &= x_{eq} + x, \\ q_T &= Q_0 + q, \end{aligned} \tag{10}$$

where x_{eq} is the equilibrium displacement and Q_0 is the charge on the bottom electrode when the system is a rest. Substituting Eq. (10) into Eqns. (8) and (9) and realizing initially x, q, and their derivatives, and f are zero allow the equilibrium points to be determined from

$$k_{eq} x_{eq} - \frac{A}{2\varepsilon_1} \left(\sigma_1 + \frac{Q_0}{A} \right)^2 = mg, \tag{11}$$

$$\frac{Q_0}{A} \left(\frac{d_1}{\varepsilon_1} + \frac{d_2}{\varepsilon_2} - \frac{x_{eq}}{\varepsilon_1} \right) + \frac{\sigma_1}{\varepsilon_1} (d_1 - x_{eq}) = 0. \tag{12}$$

Plugging the solution to Eqns. (11) and (12) yields

$$m\ddot{x} + c_{eq}\dot{x} + k_{eq} x - \frac{1}{\varepsilon_1} \left(\sigma_1 + \frac{Q_0}{A} \right) q - \frac{1}{2\varepsilon_1 A} q^2 = f, \tag{13}$$

$$R\dot{q} + \frac{q_T}{A} \left(\frac{d_1}{\varepsilon_1} + \frac{d_2}{\varepsilon_2} - \frac{x_{eq}}{\varepsilon_1} - \frac{x}{\varepsilon_1} \right) - \frac{\sigma_1 x}{\varepsilon_1} = 0. \tag{14}$$

The equivalent capacitance as function of displacement for the single dielectric generator is the inverse of the coefficient of q in

[0] In the present form of the equations of motion the surface density is related to the charge on the bottom electrode, i.e., $\sigma_{p2} A = q_T$, equivalent expression can be obtained if the top electrode is used.

Eq. (22):

$$C_s(x) = \frac{\varepsilon_1 \varepsilon_2 A}{d_1 \varepsilon_2 + (d_2 - x_{eq} - x)\varepsilon_1}. \tag{15}$$

Equations of Motion for Dual Dielectric Generator

In the dual generator the kinetic energy, and Rayleigh dissipation functions are the same as Eqns. (3) and (5). Only the potential energy changes and can be written as

$$\begin{aligned} V =& \frac{1}{2} k_{eq} x_T^2 + mg(d_2 + d_1 - x_T) \\ &+ \frac{1}{2} A \left(\varepsilon_1 E_1^2 d_1 + \varepsilon_2 E_2^2 (d_2 - x_T) + \varepsilon_3 E_3^2 d_3 \right). \end{aligned} \tag{16}$$

Applying the same procedure of applying Gausses law at the interface of each electrode and dielectric surface yields the following equations of motion

$$m\ddot{x}_T + c_{eq}\dot{x}_T + k_{eq}x_T - \frac{A}{2\varepsilon_2}\left(\sigma_2 + \frac{q_T}{A}\right)^2 = f + mg, \tag{17}$$

$$\begin{aligned} R\dot{q}_T + \frac{q_T}{A}\left(\frac{d_1}{\varepsilon_1} + \frac{d_2}{\varepsilon_2} + \frac{d_3}{\varepsilon_3} - \frac{x_T}{\varepsilon_2}\right) + \frac{\sigma_2}{\varepsilon_2}(d_2 - x_T) \\ + \frac{d_1}{\varepsilon_1}(\sigma_1 + \sigma_2) = 0. \end{aligned} \tag{18}$$

Equations around Equilibrium Points for Dual Dielectric TG

Again, the equilibrium points can be found by using Eq. (10) realizing initially x, q, their derivatives and f are zero to yield

$$k_{eq}x_{eq} - \frac{A}{2\varepsilon_1}\left(\sigma_2 + \frac{Q_0}{A}\right)^2 = mg, \tag{19}$$

$$\begin{aligned} \frac{Q_0}{A}\left(\frac{d_1}{\varepsilon_1} + \frac{d_2}{\varepsilon_2} + \frac{d_3}{\varepsilon_3} - \frac{x_{eq}}{\varepsilon_1}\right) + \frac{\sigma_2}{\varepsilon_2}(d_2 - x_{eq}) \\ + \frac{d_1}{\varepsilon_1}(\sigma_1 + \sigma_2) = 0. \end{aligned} \tag{20}$$

$$m\ddot{x} + c_{eq}\dot{x} + k_{eq}x - \frac{1}{\varepsilon_2}\left(\sigma_2 + \frac{Q_0}{A}\right)q - \frac{1}{2\varepsilon_2 A}q^2 = f, \tag{21}$$

and

$$\begin{aligned} R\dot{q} + \frac{q_T}{A}\left(\frac{d_1}{\varepsilon_1} + \frac{d_2}{\varepsilon_2} + \frac{d_3}{\varepsilon_3} - \frac{x_{eq}}{\varepsilon_2} - \frac{x}{\varepsilon_2}\right) \\ - \left(\frac{\sigma_2}{\varepsilon_2} + \frac{Q_0}{A\varepsilon_2}\right)x = 0. \end{aligned} \tag{22}$$

The equivalent capacitance as function of displacement for the dual dielectric generator is the inverse of the coefficient of q in Eq. (22):

$$C_d(x) = \frac{\varepsilon_1 \varepsilon_2 \varepsilon_3 A}{d_1 \varepsilon_2 \varepsilon_3 + (d_2 - x_{eq} - x)\varepsilon_1 \varepsilon_3 + d_3 \varepsilon_1 \varepsilon_2}. \tag{23}$$

The equations of motion for both cases can be simplified into one set of equations by defining the natural frequency (ω_n), the damping ratio, (ζ) and two lumped terms α and β:

$$\omega_n = \sqrt{\frac{k_{eq}}{m}}, \quad \text{and} \quad \zeta = \frac{c_{eq}}{2\sqrt{m k_{eq}}}. \tag{24}$$

The α and β differ for each case. In the single dielectric case they are given as:

$$\alpha = \frac{1}{\varepsilon_1}\left(\sigma_1 + \frac{Q_o}{A}\right), \quad \text{and} \quad \beta = \frac{1}{2\varepsilon_1 A}. \tag{25}$$

In the dual dielectric case they are given as:

$$\alpha = \frac{1}{\varepsilon_2}\left(\sigma_2 + \frac{Q_o}{A}\right), \quad \text{and} \quad \beta = \frac{1}{2\varepsilon_2 A}. \tag{26}$$

The simplified general equations for motion for this system for both cases can be written as:

$$\ddot{x} + 2\zeta\omega_n\dot{x} + \omega_n^2 x - \frac{\alpha}{m}q - \frac{\beta}{m}q^2 = \frac{f}{m}, \tag{27}$$

$$\dot{q} + \frac{q}{C_i(x)R} - \frac{\alpha}{R}x = 0, \quad \text{where } i = s, d. \tag{28}$$

Finally, It was found that a contact condition was necessary for when the displacement becomes equal to the initial air gap. This was done by added an extra term with a very high stiffness (k_con) to Eq. (27) when that condition is met. The new equation becomes:

$$\ddot{x} + 2\zeta\omega_n\dot{x} + \omega_n^2 x - \frac{\alpha}{m}q - \frac{\beta}{m}q^2 = \frac{f}{m}, \tag{29}$$

$$\dot{q} + \frac{q}{C_i(x)R} - \frac{\alpha}{R}x = 0, \quad \text{where } i = s, d, \quad \text{if} \quad (x < d - x_{eq}),$$

and

$$\begin{aligned} \ddot{x} + 2\zeta\omega_n\dot{x} + \omega_n^2(d - x_{eq}) \\ - \frac{\alpha}{m}q - \frac{\beta}{m}q^2 + \frac{k_{con}}{m}(x - (d - x_{eq})) = \frac{f}{m}, \end{aligned} \tag{30}$$

$$\dot{q} + \frac{q}{C_i(x)R} - \frac{\alpha}{R}x = 0, \quad \text{where } i = s, d, \quad \text{if} \quad (x < d - x_{eq}).$$

The above equations are use to simulate the performance of triboelectric device under various inputs.

NUMERICAL SIMULATONS

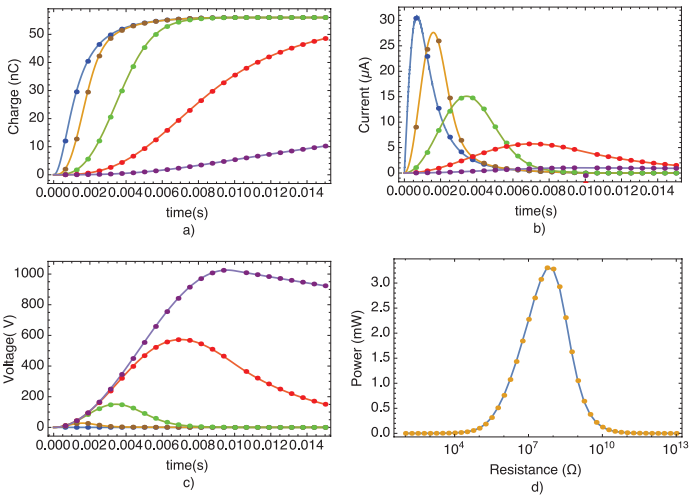

FIGURE 3. COMPARISON OF PRESENT MODEL, SOLID LINES, TO NIU [4], DOTS: A) CHARGE VS. TIME AT VARIOUS LOAD RESISTANCES, B) CURRENT VS. TIME AT VARIOUS LOAD RESISTANCES, C) VOLTAGE VS. TIME AT VARIOUS LOAD RESISTANCES, AND D) POWER VS. RESISTANCE.

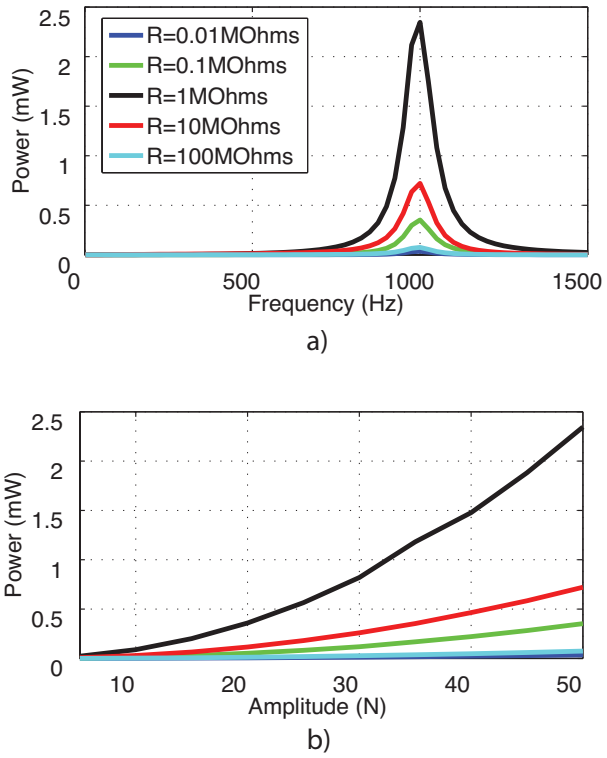

FIGURE 4. BEHAVIOR OF THE DEVICE WITH A SINE WAVE EXCITATION: (A) POWER VS. FREQUENCY AT VARIOUS RESISTANCES, AND (B) POWER VS. AMPLITUDE AT VARIOUS RESISTANCES

The single dielectric model shown in Fig. 2 was used to create and run numerical simulations created in Matlab and Simulink using ODE15s as a solver. A variety of input functions were used including a sine wave and human inputs like walking and running. Before these simulations were conducted the models were verified using a model from the literature [4] . The model that was used for verification focused only on the electrical portion of the system and assumed an equation for the displacement of the upper electrode. The comparison can be seen in Fig 3 The figures shows simulations where the mass of the TG is negligible, and the two models predictions of charge, current, voltage and power,match closely.

Periodic Functions

In order to model cyclic vibrations a sine wave was used as the forcing function. A variety of amplitudes and excitation frequencies were tested. A frequency sweep was done to determine the range of operating frequencies of the device. With only the weight of the electrode this is between 800 and 1200 Hz with the natural frequency being 996 Hz. A range of likely amplitudes was also tested to determine the optimal amplitude of excitation. This was found to be the maximum amplitude tested, 50 N. Higher amplitudes were thought to be unrealistic. Finally, the optimal resistance was found at each frequency. This was determined to be 1 MΩ for frequencies above 500 Hz and 10 MΩ for frequencies less than 500 Hz. The parameters used for the simulation are shown in Table 1 and the results are shown in Figure 5.

Human Inputs

The actions of walking and running were tested on a generator that was designed for use inside of a shoe. As a person walks or runs a load is constantly being applied and removed, therefore a discontinuous ground contact model was used to approximate the load that the device would experience as a person walks or runs [17]. The discontinuous ground contact model is given in terms of a persons weight (G), their pacing frequency (f), a Fourier coefficient (α), a phase constant (ϕ) and contact

TABLE 1. PARAMETERS USED IN THE SIMULATION WITH PERIODIC EXCITATION

Parameter	Value
Area of Electrode (A)	0.06 m^2
Thickness of Air Gap(d_1)	5.00 mm
Thickness of Dielectric (d_2)	125.00 μm
Mass of Electrode (m)	22.50 g
Equivalent Stiffness (k_{eq})	8.83×10^5N/m
Charge Density of Teflon (ρ)	30.00 C/m^3
Permittivity of Teflon (ε_1)	19.00×10^{-12} F/m
Permittivity of Air (ε_2)	8.85×10^{-12} F/m

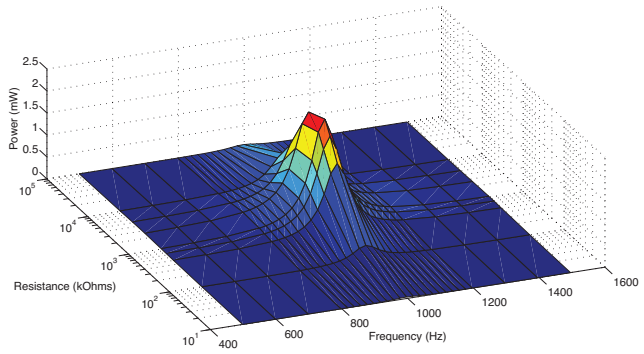

FIGURE 5. BEHAVIOR OF THE DEVICE WITH A SINE WAVE EXCITATION: POWER VS. FREQUENCY VS. RESISTANCE.

duration (t_p) as:

$$F_p = G + \sum_{i=1}^{n} \alpha_i G \cos\left(2\pi i f\left(t - \frac{t_p}{2i} - \phi_i\right)\right) \qquad (31)$$

The range of pace frequencies for each activity given in Table 2 and the corresponding Fourier coefficients in Table 3 were used in Eq. (30) to characterize the behavior of the device for walking and running. In both cases the phase constants were $\phi_1 = 0$, and $\phi_2 = \phi_3 = \pi/3$.

Time data was gathered to determine the displacement of the upper electrode and the voltage and the power generated due to this displacement. The parameters used in the simulation are shown in Table 4. The power output of this device in walking

TABLE 2. RANGE OF PACE FREQUENCY FOR VARIOUS ACTIVITIES [18]

Activity	Total Range (Hz)
Walking	1.4-2.4
Running	1.9-3.3

TABLE 3. FOURIER COEFFICIENTS [18]

Activity	Fourier Coefficients		
	α_1	α_2	α_3
Walking	0.40-0.56	0.10-0.28	0.10-0.12
Running	1.20-1.60	0.10-0.47	0.10-0.20

is on the scale of milliwatts with the maximum being 1.8 mW at the highest pacing frequency of 2.4 Hz and the optimal resistance which was 1 GΩ. The results for walking are shown in Figure 6.

TABLE 4. PARAMETERS USED IN THE SIMULATION OF WALKING AND RUNNING

Parameter	Value
Area of Electrode (A)	0.28 m^2
Thickness of Air Gap(d_1)	5.00 mm
Thickness of Dielectric (d_2)	125.00 μm
Mass of Electrode (m)	10.60 g
Equivalent Stiffness (k_{eq})	1.00×10^6N/m
Charge Density of Teflon (ρ)	30.00 C/m^3
Permittivity of Teflon (ε_1)	19.00×10^{-12} F/m
Permittivity of Air (ε_2)	8.85×10^{-12} F/m

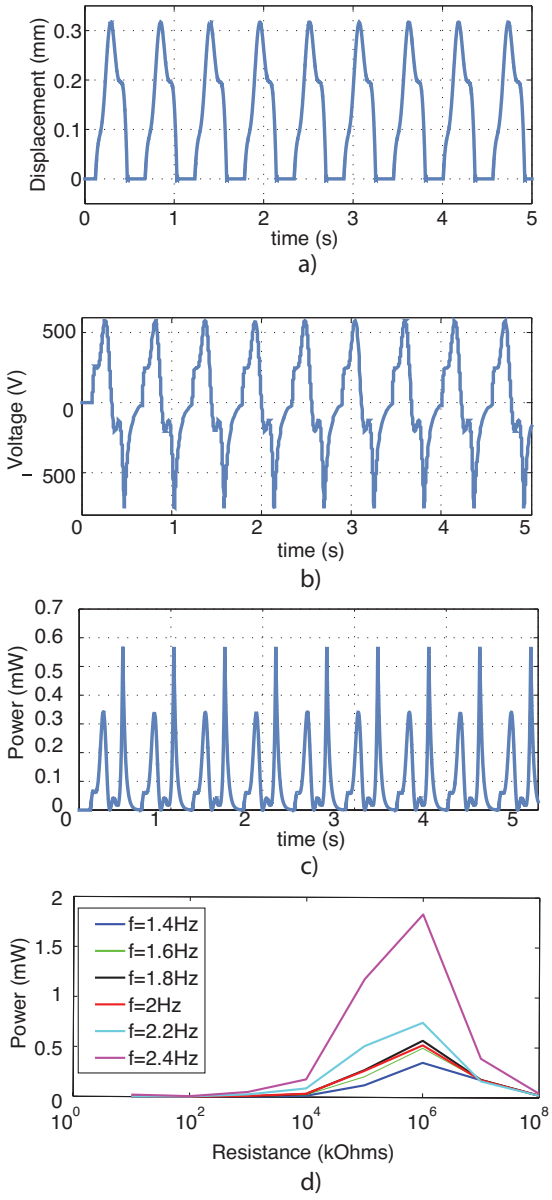

FIGURE 6. BEHAVIOR OF DEVICE IN WALKING: (A) DISPLACEMENT OF UPPER ELECTRODE VS. TIME AT 1.8 HZ AND 1 GΩ, (B) VOLTAGE VS. TIME AT 1.8 HZ AND 1 GΩ, (C) POWER VS. TIME AT 1.8 HZ AND 1 GΩ, (D) POWER VS. RESISTANCE FOR VARIOUS PACING FREQUENCIES.

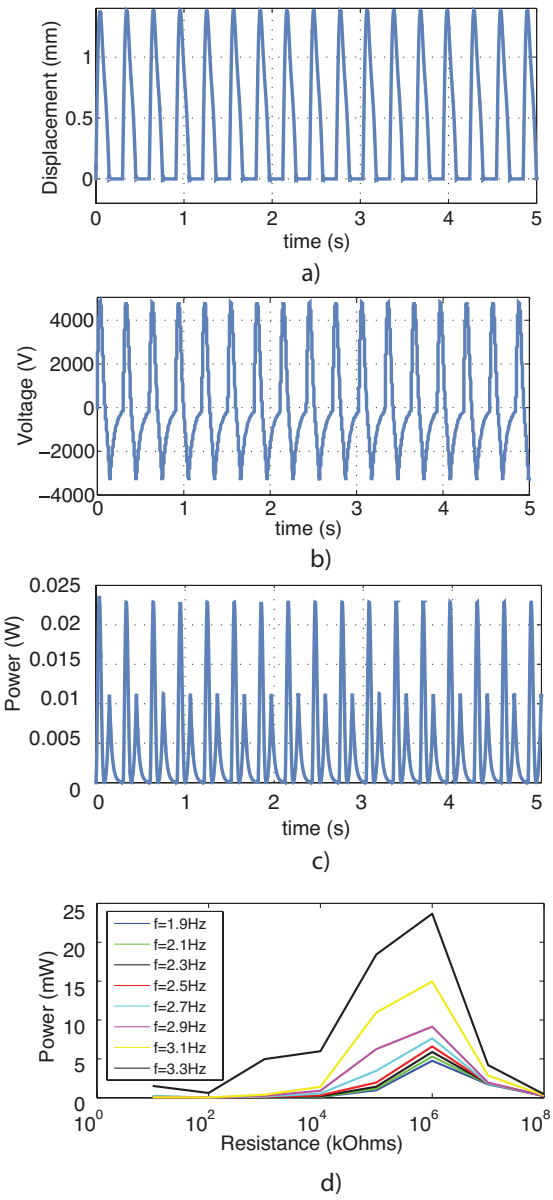

FIGURE 7. BEHAVIOR OF DEVICE IN RUNNING: (A) DISPLACEMENT OF UPPER ELECTRODE VS. TIME AT 3.3 HZ AND 1 GΩ, (B) VOLTAGE VS. TIME AT 3.3 HZ AND 1 GΩ, (C) POWER VS. TIME AT 3.3 HZ AND 1 GΩ, (D) POWER VS. RESISTANCE FOR VARIOUS PACING FREQUENCIES.

Running was also examined, again time data was gathered to determine the displacement of the upper electrode and the voltage and power generation due to that displacement. The parameters are the same as used for walking shown in Table 4 It was found that the power output increased by a factor of ten from walking to running with the maximum being 23.5 mW at the highest pace frequency of 3.3 Hz and the optimal resistance which was again found to be 1 GΩ. The results for running are shown in Fig. 7.

CONCLUSION

This paper presents a complete Lagrangian formulation of a set of electromechanical equations for contact-mode triboelectric generators. Results of simulations show that generators made from paper and thin films have an optimal operating range much higher than the low frequency applications that these generators are currently used for. The results also show that periodic excitation can result in 2.5 W of power at the optimal frequency. For walking and running which have much lower operating frequencies, the generators can produce 1.8 mW and 23.5 mW respectively. This can be greatly increased by lowering the natural frequency of the devices by adding mass or lowering the stiffness of the foam supports. Future work includes refining the model to include mechanical contact, contact resistance and forces due to volume change in an enclosed cavity for an improved generator design with an enclosed air gap. The model also needs to be refined to incorporate the nonlinear behavior of the foam supports.

ACKNOWLEDGMENT

The authors would like to thank Purdue University's Summer Undergraduate Research Fellowship Program (SURF) for their funding and support.

REFERENCES

[1] Boisseau, S., Despesse, G., and Seddik, B. A., 2012. "Electrostatic conversion for vibration energy harvesting". *arXiv preprint arXiv:1210.5191*.

[2] Roos, J., 1969. "Electrets, semipermanently charged capacitors". *Journal of Applied Physics,* ***40***(8), pp. 3135–3139.

[3] Karagozler, M. E., Poupyrev, I., Fedder, G. K., and Suzuki, Y., 2014. "Paper generators: harvesting energy from touching, rubbing and sliding". In Proc. 26th Ann. ACM Symp. User Interface Software and Technology (UIST), pp. 161–162.

[4] Niu, S., Wang, S., Lin, L., Liu, Y., Zhou, Y. S., Hu, Y., and Wang, Z. L., 2013. "Theoretical study of contact-mode triboelectric nanogenerators as an effective power source". *Energy & Environmental Science,* ***6***(12), pp. 3576–3583.

[5] Freeman, G. R., and March, N., 1999. "Triboelectricity and some associated phenomena". *Materials science and technology,* ***15***(12), pp. 1454–1458.

[6] Dhakar, L., Tay, F. E. H., and Lee, C., 2015. "Development of a broadband triboelectric energy harvester with su-8 micropillars". *Journal of Microelectromechanical Systems,* ***24***(1), pp. 91–99.

[7] Boisseau, S., Despesse, G., Ricart, T., Defay, E., and Sylvestre, A., 2011. "Cantilever-based electret energy harvesters". *Smart Materials and Structures,* ***20***(10), p. 105013.

[8] Liu, L., Towfighian, S., and Jin, Z., 2015. "A cylindrical triboelectric energy harvester for capsule endoscopes". In Biomedical Circuits and Systems Conference (BioCAS), 2015 IEEE, IEEE, pp. 1–4.

[9] Jiang, T., Zhang, L. M., Chen, X., Han, C. B., Tang, W., Zhang, C., Xu, L., and Wang, Z. L., 2015. "Structural optimization of triboelectric nanogenerator for harvesting water wave energy". *ACS nano,* ***9***(12), pp. 12562–12572.

[10] Zhong, J., Zhu, H., Zhong, Q., Dai, J., Li, W., Jang, S.-H., Yao, Y., Henderson, D., Hu, Q., Hu, L., et al., 2015. "Self-powered human-interactive transparent nanopaper systems". *ACS nano,* ***9***(7), pp. 7399–7406.

[11] Zhang, L., Xue, F., Du, W., Han, C., Zhang, C., and Wang, Z., 2014. "Transparent paper-based triboelectric nanogenerator as a page mark and anti-theft sensor". *Nano Research,* ***7***(8), pp. 1215–1223.

[12] Fan, X., Chen, J., Yang, J., Bai, P., Li, Z., and Wang, Z. L., 2015. "Ultrathin, rollable, paper-based triboelectric nanogenerator for acoustic energy harvesting and self-powered sound recording". *ACS nano,* ***9***(4), pp. 4236–4243.

[13] Yang, P.-K., Lin, Z.-H., Pradel, K. C., Lin, L., Li, X., Wen, X., He, J.-H., and Wang, Z. L., 2015. "Paper-based origami triboelectric nanogenerators and self-powered pressure sensors". *ACS nano,* ***9***(1), pp. 901–907.

[14] Jin, C., Kia, D. S., Jones, M., and Towfighian, S., 2016. "On the contact behavior of micro-/nano-structured interface used in vertical-contact-mode triboelectric nanogenerators". *Nano Energy,* ***27***, pp. 68–77.

[15] Niu, S., Liu, Y., Zhou, Y. S., Wang, S., Lin, L., and Wang, Z. L., 2015. "Optimization of triboelectric nanogenerator charging systems for efficient energy harvesting and storage". *IEEE Transactions on Electron Devices,* ***62***(2), pp. 641–647.

[16] Hawley, M. S., and Romanow, F. F., 1978. "Electret transducer equations by lagrange?s equation". *The Journal of the Acoustical Society of America,* ***64***(2), pp. 694–696.

[17] Bachmann, H., and Ammann, W., 1987. *Vibrations in structures: induced by man and machines*, Vol. 3. Iabse.

[18] Hoorpah, W., 2002. Vibration of footbridges under pedestrian loads.